  DOI 10.1515/HTMP.2011.108

Hot-dip Aluminizing Fabrication of $TiAl_3$ Coating on TA15 Alloy and Its High Temperature Oxidation Behaviors

Z. G. Zhang,[1,*] Y. P. Peng,[1] Y. L. Mao,[1] C. M. Hou[1] and L. Xu[2]

[1] School of Applied Chemistry, Shenyang University of Chemical Technology, Shenyang, China

[2] Institute of Metal Research, Chinese Academy of Sciences, Shenyang, China

Abstract. A $TiAl_3$-rich coating was developed by hot-dip aluminizing method and subsequent interdiffusion treatment on Ti-6.5Al-1Mo-1V-2Zr (mass %) alloy for high temperature resistance. Interrupted oxidation at temperatures from 973 to 1173 K and isothermal oxidation at temperatures from 923 to 1073 K of the $TiAl_3$-rich coating were conducted. The coating markedly decreased the oxidation rate in comparison with the substrate alloy at 1073 K and lower during the interrupted oxidation, and a layered structure of $Al_2O_3/TiAl_3/TiAl_2/TiAl$/alloy from the outside to the inside formed after oxidation at 973 K without changing the main body of the $TiAl_3$-rich coating. The oxidation kinetics followed parabolic relations during the stable state stage of the isothermal oxidation; the activation energy for oxidation of the coating was calculated as 323 kJ mol^{-1}. The hot-dip aluminizing coating provided high protectiveness for the Ti-6.5Al-1Mo-1V-2Zr alloy at 973 K and lower. The oxidation performance of the $TiAl_3$-rich coating was discussed in detail.

Keywords. Ti-6.5Al-1Mo-1V-2Zr, high temperature oxidation, hot-dip aluminizing, activation energy.

PACS®(2010). 81.65.Mq.

1 Introduction

Ti-based TA15 alloy with nominal composition of Ti-6.5Al-1Mo-1V-2Zr (mass %) is a near-α Ti-alloy of high aluminum equivalent. TA15 possesses medium strength at high-temperature, good thermal stability, and excellent weldability; TA15 is comparable to Ti-8Al-1Mo-1V (Ti811), and has been widely used as structural materials in aero-industries [1–3]. However, the insufficient oxidation resistance is one of the main factors that limit the applications of TA15 at high temperatures, and this alloy is designed for working under 773 K [3]. Ti-based alloys degrade quickly during oxidation at high temperatures because of the formation of non-protective oxide scale [4–7]. In addition, oxygen embrittlement of the Ti-based alloys occurs during exposures to oxidizing environments [4]. Therefore, it is necessary to introduce some surface modifications to enhance the high temperature oxidation resistance of Ti-based alloys, including TA15, without altering the bulk properties.

In addition to the methods of surface alloying [7–9], the most commonly used method for improving the oxidation resistance of Ti-based alloys (excluding Ti-Al intermetallics) is the fabricating of diffusion barrier coatings, which includes evaporating or sputter-deposition [4, 6], pack aluminization and electrodepositing [10], thermal spray [11], plasma-spray process [12, 13], pulsed bi-polar micro-plasma oxidation [14], halide-activated pack cementation and arc ion plating [15], vitreous enamel coating [16, 17], and magnetron sputtering [18].

Besides the above mentioned processes for developing protective coatings, hot-dip aluminizing should be an applicable method for protection of Ti-based alloys against high temperature oxidation since hot-dip galvanization is a traditional and reliable commercial method for protection of steel against corrosion [19]. In fact, a $TiAl_3$-rich coating has been successfully developed on a γ-TiAl alloy through hot-dip aluminizing and subsequent interdiffusion treatment [20], and the oxidation resistance at high temperatures of the alloy was significantly improved due to the developed $TiAl_3$-rich coating [21]. The microstructure and oxidation of hot-dip aluminized titanium at high temperature [22] and the effect of Ni, Si, and Cr in the structural formation of diffusion aluminide coatings on commercial-purity titanium [23] were also reported.

In the present work, hot-dip aluminizing and subsequent interdiffusion treatment were used to develop a $TiAl_3$ coating on a commercial TA15 alloy, and the oxidation behaviors at high temperatures of the coating were studied.

2 Material and Methods

2.1 Hot-dip Aluminizing

The material studied is commercial TA15 alloy with nominal composition of Ti-6.5Al-1Mo-1V-2Zr (mass %). The coupons with dimensions of $20 \times 10 \times 2$ mm were cut from

* **Corresponding author:** Z. G. Zhang, School of Applied Chemistry, Shenyang University of Chemical Technology, 110142, Shenyang, China; E-mail: zhg_syict@sohu.com.

Received: January 28, 2011. Accepted: April 16, 2011.

the TA15 alloy with a spark line saw, and a hole of 1.5 mm diameter was made on each sample near the edge for suspension purpose. All the specimens were mechanically abraded on successively finer abrasive papers up to 1000 grit, and were subsequently cleaned with water, acetone, and ethanol, and then were dried immediately.

Prior to the hot-dip aluminizing, the specimens were treated with an acid pickling solution containing 5 vol.% HF and 10 vol.% HNO_3 for 10–15 s followed by washing in water and ethanol, and then were dried. A mixture of KCl, NaCl, and NaF with the mole ratio of 4 : 3 : 1 was used to cover the molten Al in advance. The molten Al bath was kept at 993 K under argon atmosphere, and the treated specimens were vertically immersed into the bath for 15 s. The speed of immersion and retreat was about 0.05 $m \cdot s^{-1}$. The hot-dip aluminized specimens after retreat were first thrown into water at room temperature to remove the impurities attached to the surface, and were further washed in water and ethanol, and then were dried. The interdiffusion treatment of the aluminized specimens was carried out at 873 K in laboratory air for 30 h (1 h = 3600 s), after which the specimens were covered by an overlay of Ti-Al compounds referred to as "coating/TA15" in the following text.

To minimize the experimental error resulted from the thickness inhomogeneity of the coating/TA15 during isothermal oxidation, the specimens to be isothermally oxidized were given special treatment by carefully grinding off the excess Al on the thick parts after the hot-dip aluminizing, and then the interdiffusion treatment was carried out.

2.2 Oxidation Tests

The oxidation properties of the TA15 alloy and the coating/TA15 were examined at temperatures between 973 and 1173 K in the laboratory air using interrupted oxidation. The interrupted oxidation was conducted in a muffle furnace up to 300 h. After putting a specimen into an Al_2O_3 crucible, the oxidation tests were started by introducing the crucible directly into the hot furnace to ensure rapid heating-up. The mass changes were measured at increasingly large intervals after removing the Al_2O_3 crucible together with the specimen from the furnace and cooling in the air. The cooling time was set at 25 min (1 min = 60 s) to decrease the experimental error, and only the specimen was measured for the mass changes.

The isothermal oxidations for the coating/TA15 at temperatures between 923 and 1073 K were conducted by using a thermobalance. The surface areas of the specimens were measured firstly, and then a specimen was suspended with a quartz filament in the hot zone of the furnace attached to the thermobalance. The weight change of the specimen was continuously recorded.

2.3 Microstructure Examination

The phase analyses of the TA15 alloy and the coating/TA15 were conducted by using X-ray diffraction (XRD) from the surface. The target material used in the X-ray diffractometer, Bruker D8, is copper (Cu). The electric current of 40 mA and voltage of 40 kV were used in the XRD analysis. Also, the surface of the coating/TA15 before oxidation was examined by using a scanning electron microscope (SEM, JEOL JSM-6360LV) under second electron image (SEI). Some of the specimens were mounted in the cold-setting epoxy resin to examine the cross-section in the SEM under backscattered electron image (BEI), and the distributions of elements in the various solid phases were analyzed by using an energy dispersive X-ray spectroscope (EDS) attached in the SEM.

The XRD analysis was performed on the oxidized specimens without stripping the oxide film. The cross-sections of the oxidized specimens were examined as described above.

3 Results and Discussion

3.1 Development of the $TiAl_3$-rich Coating/TA15

The micrograph of the cross-section of the TA15 alloy after hot-dip aluminizing is shown in Figure 1, which indicates that a surface coating of pure Al was formed. Between the pure Al coating and the substrate there is a thin diffusion layer with a uniform thickness of less than 0.5 μm. The thickness of the pure Al coating is nonuniform everywhere. When the specimen was pulled out of the molten Al bath, the coating near the bottom edge of the specimen was much thicker than the coating on the other places. The thickness of the coatings ranged from 20 μm at the center part to 80 μm at the bottom edge of the specimens. None embrittlement cracking of the pure Al coating was found, after water quenching, which should be attributed to the good ductility of Al metal. TA15 is a dual-phase alloy containing α and β phase [1–3], which coincides with the two-phase microstructure shown in Figure 1, i.e. the prevailing α-phase and the bright β-phase.

After the interdiffusion treatment at 873 K for 30 h, the micrographs of the cross-section of the coating/TA15 are shown in Figure 2, which displays a uniform single-phase surface coating; the average atom ratio of Ti versus Al is 1 : 3.7 (uncorrected, the same below). A few through-thickness cracks, perpendicular to the alloy surface, were occasionally found in the coating/TA15. The formation of these cracks should be attributed to the tensile stresses generated due to the mismatch in the coefficients of thermal expansion (CTE) between the coating and the substrate alloy during the cooling from the interdiffusion treatment temperature to the room temperature.

The surface XRD patterns of the TA15 alloy and the coating/TA15 before oxidation are shown in Figure 3. The

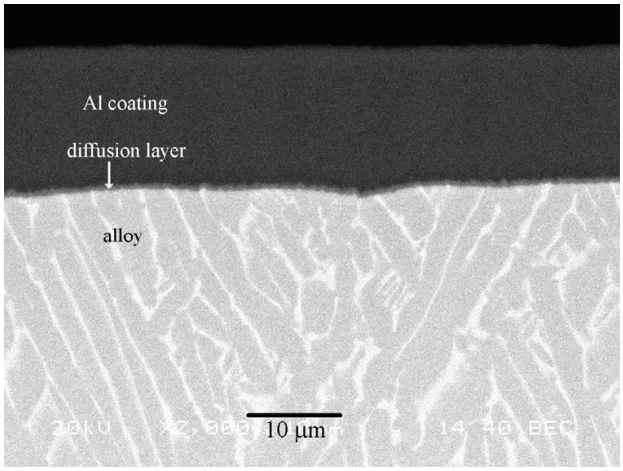

Figure 1. Micrograph of cross-section of the TA15 alloy after hot-dip aluminizing.

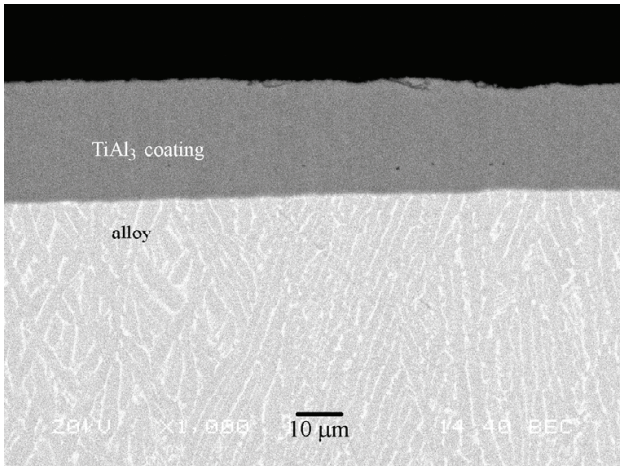

Figure 2. Micrograph of cross-section of the coating/TA15.

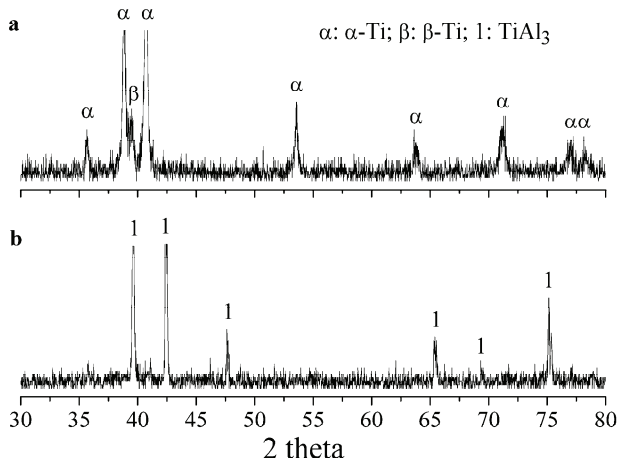

Figure 3. Surface X-ray diffraction patterns before oxidation. a – the TA15 alloy; b – the coating/TA15.

α-phase is the dominant microstructure in the TA15 alloy (Figure 3a), and only one weak signal of β-phase was detected, which is consistent with the cross-section morphology of the TA15 alloy shown in Figure 1. By combining the EDS and the XRD analysis (Figure 3b), it is identified that the coating/TA15 developed on the TA15 alloy after the interdiffusion treatment is composed of $TiAl_3$ phase. The content of hybrid phase, such as retained Al and alumina formed during the interdiffusion treatment, on the surface of the coating/TA15 is low with respect to the detection limit of the XRD analysis. According to the Ti-Al phase diagram [24], four intermetallic compounds, namely Ti_3Al, TiAl, $TiAl_2$, and $TiAl_3$, could be formed during the solid state reaction between Ti and Al. However, only one of the four products will be obtained below the melting point of Al at constant pressure, according to the phase rule, if Ti and Al exist at the same time. The published experiments on Ti-Al diffusion systems in the solid state also showed that $TiAl_3$ is the only compound formed during reaction between Ti and Al [25–27]. The free energy of formation of $TiAl_3$ has been found to be the lowest among the compounds Ti_3Al, TiAl, and $TiAl_3$ in the temperature range from 273 to 1473 K [28], so the formation of Ti_3Al and/or TiAl is ruled out from thermodynamic considerations. However, $TiAl_2$ has slightly lower free energy of formation compared to that of $TiAl_3$ [28], so the reaction kinetics mechanism should be taken into account for the absence of $TiAl_2$. The published activation energies of formation of $TiAl_3$ for the reaction $Ti + 3Al = TiAl_3$ and TiAl-Al diffusion couple are 170.5 kJ mol^{-1} [29] and 95 kJ mol^{-1} [25], respectively, which are smaller than the activation energy (240 kJ mol^{-1}) of growth of $TiAl_2$ in TiAl-$TiAl_3$ diffusion couple and the activation energy (206 kJ mol^{-1}) of growth of Ti_3Al-TiAl-$TiAl_2$ in Ti-$TiAl_3$ diffusion couple [25]. These data support that the product in Ti-Al system is $TiAl_3$ than $TiAl_2$ at a relatively lower temperature.

3.2 Effect of the Coating/TA15 on the High Temperature Oxidation Resistance

The interrupted oxidation kinetic curves of the TA15 alloy and the coating/TA15 at 973 and 1073 K in air are shown in Figure 4(a), and the curves at 1173 K are separately shown in Figure 4(b) because the oxidation rate of coating/TA15 is high at this temperature. At temperatures of 973 and 1073 K, the oxidation rates of the TA15 alloy are significantly reduced because of the existence of the coating/TA15. The TA15 alloy quickly degraded when oxidized at 1073 K; apparent spallation of the surface oxides occurred after about 30 h, and breakaway oxidation occurred after 40 h. The oxidation kinetic curve of the coating/TA15 at 1073 K is similar to that of the TA15 at 973 K, i.e. the mass slowly increases with time showing an approximate linear relation between the mass gain and oxidation time

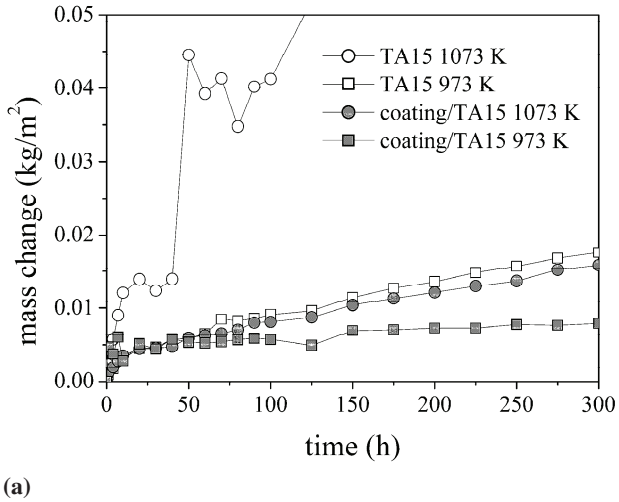

(a)

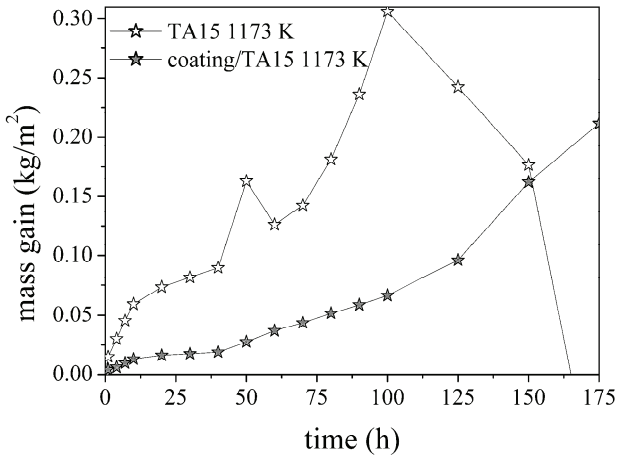

(b)

Figure 4. The interrupted oxidation kinetic curves, mass gain versus time, of the TA15 alloy and the coating/TA15 at high temperatures in air. (a) 973 and 1073 K; (b) 1173 K.

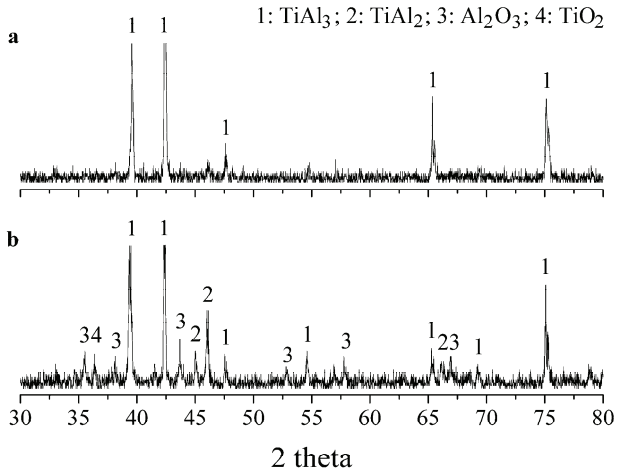

Figure 5. Surface X-ray diffraction patterns of the coating/TA15 after interrupted oxidation for 300 h in air. a – 973 K; b – 1073 K.

after about 75 h. The oxidation curve of the coating/TA15 at 973 K shows a typical character of protective oxidation after a short transient stage of about 10 h. The weight loss in general was not found during the oxidation of the coating/TA15 (excluding the transient stage) at both temperatures, but slight spallation of the surface oxides occasionally occurred when the specimen was taken out of the muffle furnace and cooled. The oxides spallation resulted in the fluctuation of the mass change curves as shown in Figure 4(a).

Both the TA15 alloy and the coating/TA15 oxidized quickly at 1173 K. Breakaway oxidation of the alloy occurred after about 40 h, and then severe spallation of the surface oxides occurred. Weight loss in comparison with the original weight was recorded after 175 h for the alloy. The curve of the coating/TA15 shows a step-type oxidation process (Figure 4(b)); the coating/TA15 failed to maintain the protective oxidation all the time, and two accelerations of oxidation occurred at about 40 h and 125 h, respectively. Although the weight loss was not found during the oxidation, the deformation of the specimens was apparent, and the surface oxides spalled continuously, which indicates that the coating/TA15 is not able to provide oxidation protection for the TA15 alloy at 1173 K and higher. In addition, the linear relation between the mass gain and oxidation time of the coating/TA15 at 1073 K (Figure 4(a)) implies that the oxidation protection provided for the TA15 alloy at 1073 K is not reliable in the case of long term oxidation. For $TiAl_3$ intermetallic, the maximum temperature of oxidation resistance is about 1273 K [30], but this would be discounted if $TiAl_3$ is coated on an alloy, such as TA15, lacking in oxidation resistance at high temperatures. When $TiAl_3$ is used as a protective coating on TA15, interdiffusion between $TiAl_3$ and the substrate inevitably occurs during exposure in high temperature environments. In such a condition, $TiAl_3$ is consumed not only by oxidation of itself but also by the growth of possible solid state reaction products such as $TiAl_2$, TiAl, and Ti_3Al, which are not as oxidation resistant as $TiAl_3$.

Figure 5 shows the surface XRD patterns of the coating/TA15 after interrupted oxidation for 300 h at 973 and 1073 K. Only diffraction peaks of $TiAl_3$ phase were identified after the oxidation at 973 K (Figure 5a), which indicates that the coating/TA15 developed on the TA15 alloy is stable at this temperature and the content of the main product, Al_2O_3, during oxidation is low. On the contrast, the XRD patterns shown in Figure 5b illustrate that quite a bit of $TiAl_3$ phase in the coating/TA15 degraded into $TiAl_2$ phase after the 1073 K interrupted oxidation and the main oxidation product is Al_2O_3.

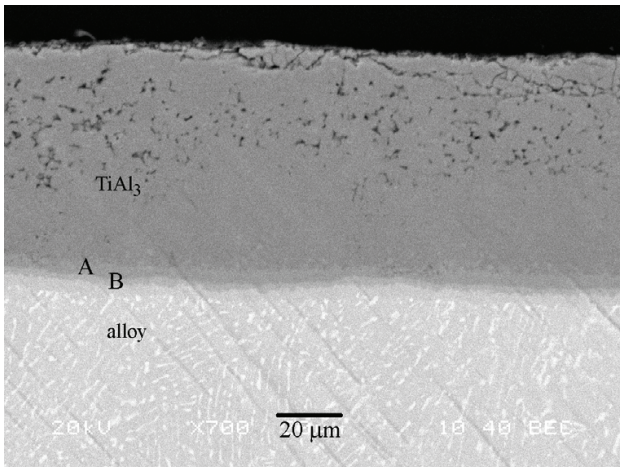

(a)

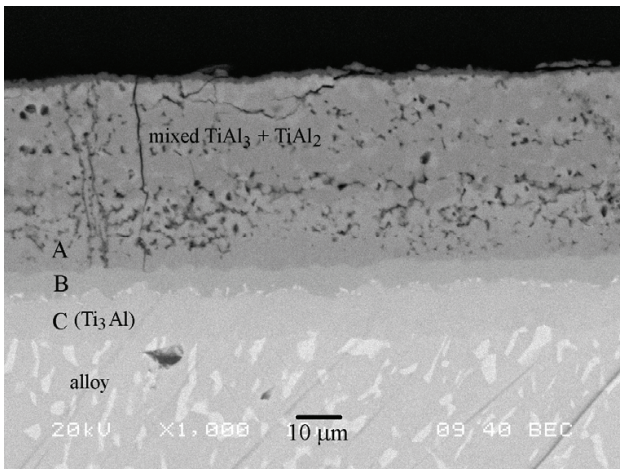

(b)

Figure 6. Micrographs of cross-section of the coating/TA15 after interrupted oxidation for 300 h in air. (a) 973 K; (b) 1073 K. A represents $TiAl_2$, and B represents TiAl.

The micrographs of cross-section of the coating/TA15 after interrupted oxidation for 300 h at 973 and 1073 K are shown in Figure 6, which reveals that the coating/TA15 developed a layered structure after the oxidation. A thin layer of Al-rich oxide formed at the interface between the coating/TA15 and air (the Al-rich layer is much thinner at 973 K). According to Figure 6(a), two diffusion layers (marked as A and B) formed at the interface between the coating/TA15 and substrate, but the main body of the coating/TA15 is unchanged. It was determined that the layer A and layer B were composed of $TiAl_2$ and TiAl by studying the EDS results (average atom ratios of Ti versus Al are 1 : 2.4 and 1 : 1.5 of layer A and B, respectively). The formation of the micro-pores in the upper part of the coating/TA15 should be attributed to the consumption of Al through outwards diffusion.

Figure 6(b) reveals that the coating/TA15 degraded seriously after the oxidation at 1073 K although a layer of Al-rich oxide formed on the coating/TA15 surface; no distinct $TiAl_3$ layer was left, but a layer of mixed $TiAl_3$ and $TiAl_2$ formed just beneath the Al_2O_3-rich layer. Three diffusion layers (marked as A, B, and C) formed at the interface between the mixed layer and substrate. The layer of mixed $TiAl_3$ and $TiAl_2$ is full of micro-pores, and the internal oxidation of Al extensively occurred in the layer A. This suggests that the outwards diffusion of Al and inwards diffusion of O_2 were greatly strengthened during the oxidation at 1073 K. The composition of layer A and layer B in Figure 6(b) is the same as that of A and B marked in Fig.6a. The layer C was identified as Ti_3Al with an average atom ratio of Ti versus Al of 2.6 : 1. The layer C is much thicker than the layer B, which is different from the thickness relation between the layers A and B at 973 K (Figure 6(a)). This heavy interdiffusion between the coating/TA15 and substrate implies that the coating/TA15 is not able to provide long-term oxidation resistance for the TA15 alloy at 1073 K in spite of the formation of protective Al_2O_3-rich layer during the 300 h oxidation. Breakaway oxidation will occur, sooner or later, if the coating/TA15 is degraded because of the double consumption of $TiAl_3$ by oxidation and interdiffusion.

In addition, the through-thickness cracks occasionally formed in the coating/TA15 after the interdiffusion treatment did not propagate during the oxidation and no fast degradation near the cracks was found (Figure 6(b)). This is in contrast to the results, concerning the cracks effect on the oxidation performance of diffusion coatings on Ti-based alloy [10] and of thick $TiAl_3$ coatings [31], have been reported. Pack aluminization process was used in Ti-based IMI-834 alloy [10] and Ti_3Al-Nb [31], and both of them reported that the cracks propagated and led to drastic substrate degradation during the oxidation. In fact, it is reasonable to expect that the propagation or development of the cracks will be undercut when the transitional diffusion layers, such as $TiAl_2$, TiAl, and Ti_3Al, are formed. This kind of gradational structure will decrease the mismatch in CTE between the coating and the substrate alloy.

It was failed to characterize the oxidation kinetics due to the spallation of oxides occurred during the interrupted oxidation. The isothermal oxidation of the coating/TA15 at temperatures from 923 to 1073 K, followed by the continuously recording the mass change with a thermobalance, was therefore carried out. Figure 7 shows the isothermal oxidation kinetic curves of mass changes versus time and of mass changes versus square root of time. Evidently, the mass gains recorded during the stable state oxidation stage were parabolic with respect to time, which suggests that the rate-limiting step might be diffusion related. These parabolic stages and the corresponding parabolic rate constants (k_p) are given in Table 1. Both the XRD analysis (Figure 5) and the examination of the cross-section of the oxidized

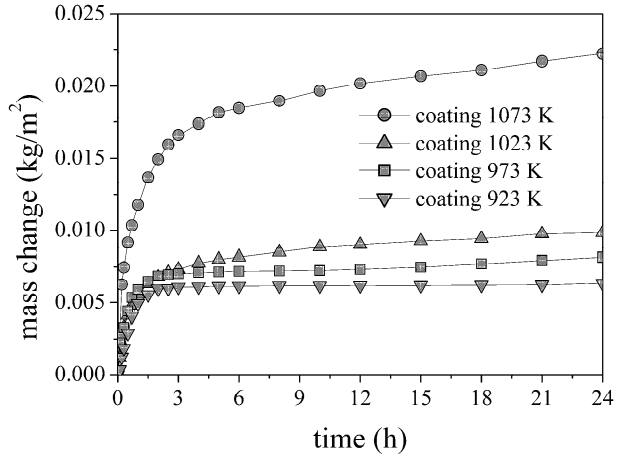

(a)

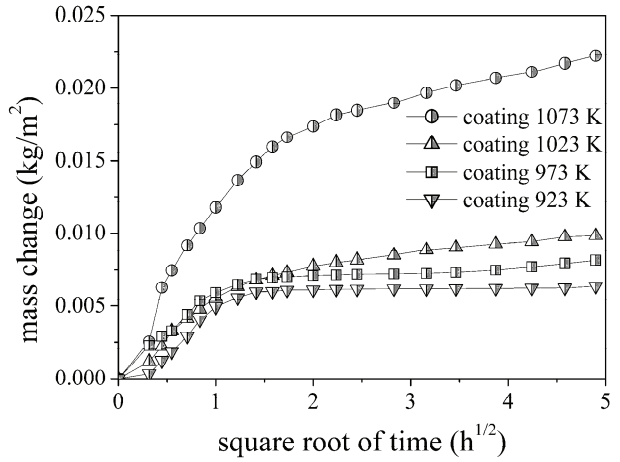

(b)

Figure 7. The isothermal oxidation kinetic curves of the coating/TA15 at temperatures from 923 to 1073 K in air. (a) mass gain versus time; (b) mass gain versus square root of time.

Temperature (K)	Oxidation duration (h)	k_p (kg^2 m^{-4} s^{-1})
923	2–24	1.8×10^{-12}
973	2–24	2.8×10^{-11}
1023	4–24	1.4×10^{-10}
1073	4–24	7.0×10^{-10}

Table 1. Parabolic rate constants for the isothermal oxidation of the coating/TA15 in air.

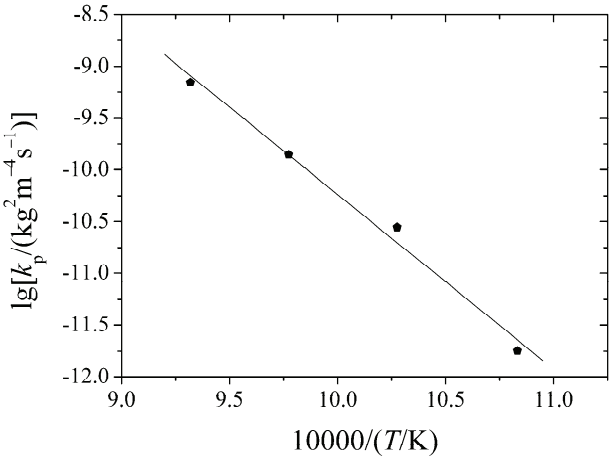

Figure 8. Arrhenius plot for the parabolic rate constants of the coating/TA15 at temperatures from 923 to 1073 K in air.

coating/TA15 (Figure 6) reveal that protective Al_2O_3-rich oxides scale formed during the oxidation, but the rate constants are two orders of magnitude higher than the typical values of alumina growth on NiAl or FeAl intermetallics [32] at the same oxidation temperatures. It was suggested that this abnormally high oxidation rates result from the existence of Al metal as a second phase in the microstructure of $TiAl_3$ coating [30]. According to the systematic studies of the oxidation kinetics, in the temperature range from 973 to 1473 K, of cast $TiAl_3$ intermetallic [30], the oxidation rate of $TiAl_3$ at temperatures below 1273 K is considerably higher than classical alumina growth and actually approach TiO_2 kinetics although the surface scales were identified as Al_2O_3. The "abnormal oxidation kinetics" characterized by the higher k_p might attribute to the formation of micropores in the coating/TA15 investigated in the present work. These micro-pores lead to an increase of oxidation surface area. The formation of the micro-pores was also reported in the diffusion couple of solid Ti and molten Al [33], which might be resulted from the asymmetric diffusion during the interdiffusion treatment at high temperatures. The asymmetric diffusion means that the vacancies left after diffusion of Al was not able to be filled by other species.

Dependence of $\log(k_p)$ on reciprocal of absolute temperature is plotted in Figure 8, which displays a linear relation between $\log(k_p)$ and $1/T$. According to Arrhenius equation, the activation energy E_a of oxidation is calculated as 323 kJ mol^{-1}. The oxidation process is diffusion-controlled if the protective oxide scale is formed, and the E_a of oxidation reaction should be equivalent to that of diffusion. However, differences in the experimental methods, conditions, and samples resulted in large scatter of the E_a. The E_a of this study is much higher than that (about 225 kJ mol^{-1}) calculated for pack aluminization coatings on IMI-834 alloy [10] under cyclic oxidation, but is somewhat lower than that (about 338 kJ mol^{-1}) calculated for oxygen diffusion in alumina layer formed on $TiAl_3$ [34].

4 Conclusion

Hot-dip aluminizing method and subsequent interdiffusion treatment were used to develop a $TiAl_3$-rich coating on Ti-6.5Al-1Mo-1V-2Zr alloy. The $TiAl_3$ coating markedly decreased the oxidation rate in comparison with the alloy at 1073 K and lower during the interrupted oxidation; the oxidation kinetics followed parabolic relations during the stable state oxidation stages at temperatures between 923 and 1073 K. The activation energy for oxidation of the coating was found to be 323 kJ mol^{-1}.

A layered structure of $Al_2O_3/TiAl_3/TiAl_2/TiAl$/alloy from the outside to the inside formed after oxidation at 973 K without changing the main body of the $TiAl_3$ coating. On the contrary, a layered structure of $Al_2O_3/(TiAl_3+TiAl_2)/TiAl_2/TiAl/Ti_3Al$/alloy formed after oxidation at 1073 K. The hot-dip aluminizing $TiAl_3$ coating provided high protectiveness for the Ti-6.5Al-1Mo-1V-2Zr alloy against oxidation at 973 K and lower.

References

[1] A. X. Sha, X. W. Li and J. P. Chu, *Chin. J. Rare Met.*, **27** (2003), 213–215.

[2] W. C. Xu, D. B. Shan, Y. Lv and C. F. Li, *J. Mater. Sci. Technol.*, **21** (2005), 807–812.

[3] Y. L. Wang and G. S. Wang, *Chin. J. Rare Met.*, **22** (1998), 152–154.

[4] R. K. Clark, J. Unnam and K. E. Wiedemann, *Oxid. Met.*, **29** (1988), 255–269.

[5] H. L. Du, P. K. Datta, D. B. Lewis and J. S. Burnell-Gray, *Corros. Sci.*, **36** (1994), 631–642.

[6] H. L. Du, P. K. Datta and J. S. Burnell-Gray, *J. Mater. Sci.*, **30** (1995), 2640–2647.

[7] A. Y. Fasasi, S. K. Roy, A. Galerie, M. Pons and M. Caillet, *Mater. Lett.*, **13** (1992), 204–211.

[8] W. B. Wang, Z. Xu, Z. Y. He, Z. X. Wang and P. Z. Zhang, *Key Eng. Mater.*, **353–358** (2007), 1818–1821.

[9] Y. S. Tian, Q. Y. Zhang and D. Y. Wang, *J. Mater. Process. Technol.*, **209** (2009), 2887–2891.

[10] Md. Zafir Alam and Dipak K. Das, *Corros. Sci.*, **51** (2009), 1405–1412.

[11] Z. W. Li, W. Gao, D. Y. Ying and D. L. Zhang, *Scripta Mater.*, **48** (2003), 1649–1653.

[12] D. W. McKee and K. L. Luthra, *Surf. Coat. Technol.*, **56** (1993), 109–117.

[13] B. Y. Choi, J. Liang and W. Gao, *Met. Mater. Int.*, **11** (2005), 499–503.

[14] G. D. Hao, Z. H. Jiang, Z. P. Yao, H. Z. Xian and Y. L. Jiang, *Key Eng. Mater.*, **336–338** (2007), 2481–2483.

[15] X. M. Peng, C. Q. Xia, Y. Y. Liu and Z. G. Zhang, *Rare Met.*, **28** (2009), 49–56.

[16] Y. M. Xiong, S. L. Zhu, F. H. Wang and C. H. Lee, *J. Coat. Tech. Res.*, **5** (2008), 93–98.

[17] Y. M. Xiong, F. H. Wang, W. T. Wu and Y. Niu, *Mater. Sci. Forum*, **369–372** (2001), 743–750.

[18] C. Leyens, J.-W. van Liere, M. Peters and W. A. Kaysser, *Surf. Coat. Technol.*, **108-109** (1998), 30–35.

[19] S. M. A. Shibli, R. Manu and V. S. Dilimon, *Appl. Surf. Sci.*, **245** (2005), 179–185.

[20] Z. G. Zhang, X. Teng, H. F. Xiang, Y. G. Sheng and X. J. Zhang, *High Temp. Mater. Processes*, **28** (2009), 115–119.

[21] Z. G. Zhang, X. Teng, Y. L. Mao, C. X. Cao, S. J. Wang and L. Wang, *Oxid. Met.*, **73** (2010), 455–466.

[22] D. Q. Wang, Z. Y. Shi and Y. L. Teng, *Appl. Surf. Sci.*, **250** (2005), 238–246.

[23] G. P. Cammarota, A. Casagrandea and G. Sambogna, *Surf. Coat. Technol.*, **201** (2006), 230–242.

[24] T. B. Massalski, *Binary Alloys Phase Diagrams*, second ed., ASM International, The Materials Information Society, Ohio USA (1996).

[25] F. J. J. Van Loo and G. D. Rieck, *Acta Metall.*, **21** (1973), 61–84.

[26] S. Wöhlert and R. Bormann, *J. Appl. Phys.*, **85** (1999), 825–832.

[27] E. K. Y. Fu, R. D. Rawlings and H. B. McShane, *J. Mater. Sci.*, **36** (2001), 5537–5542.

[28] M. Sujata, S. Bhargava and S. Sangal, *J. Mater. Sci. Lett.*, **16** (1997), 1175–1178.

[29] T. Wang, R. Y. Liu, M. L. Zhu and J. S. Zhang, *J. Therm. Anal. Calorim.*, **70** (2002), 507–519.

[30] J. L. Smialek and D. L. Humphrey, *Scr. Metall. Mater.*, **26** (1992), 1763–1768.

[31] J. L. Smialek, *Corros. Sci.*, **35** (1993), 1199–1208.

[32] H. J. Grabke, *Intermetallics*, **7** (1999), 1153–1158.

[33] A. A. Abdel-Hamid, *Z. Metallkunde*, **82**, 921-927 (1991).

[34] R. G. Reddy, X. Wen and I. C. I. Okafor, *Metall. Mater. Trans.*, **31A** (2000), 3023–3028.